Published by Avanti Publishers

Journal of Advanced Thermal Science Research

ISSN (online): 2409-5826

Comparison of Volume Average and Pore Scale Methods for a Square Cavity with Thin Vertical Porous Layer under Mixed Convection Heat Transfer

Naoya Tazawa[1], Kou Miyazaki[1], Chunyang Wang[2] and Moghtada Mobedi[1,*]

[1]*Mechanical Engineering Course, Graduate School of Integrated Science and Technology, Shizuoka University, Hamamatsu City 432-8561, Japan*

[2]*Institute of Engineering Thermophysics, Chinese Academy of Sciences, Beijing 100190, China*

ARTICLE INFO

Article Type: Research Article

Academic Editor: Wen-Zhen Fang

Keywords:
Pore scale method
Thin porous media
Volume average method
Heat transfer in porous media

Timeline:
Received: March 24, 2025
Accepted: May 05, 2025
Published: May 30, 2025

Citation: Tazawa N, Miyazaki K, Wang C, Mobedi M. Comparison of volume average and pore scale methods for a square cavity with thin vertical porous layer under mixed convection heat transfer. J Adv Therm Sci Res. 2025; 12: 1-20.

DOI: https://doi.org/10.15377/2409-5826.2025.12.1

ABSTRACT

The problem of heat and fluid flow through a vertical thin porous medium located in an open square cavity is considered. This problem is analyzed using two approaches: the Pore Scale Method (PSM) and the Volume Average Method (VAM), for different Reynolds and Richardson numbers. The dimensional and dimensionless governing equations for both methods are presented. The velocity and temperature distributions obtained from the two approaches are compared to determine the range of Darcy numbers (i.e., the number of pores in the vertical direction) for which the results of the volume average approach can be validated. The obtained results indicated a good agreement between the velocity and temperature distributions of the two methods when the number of pores in vertical direction is approximately 20. However, decreasing the number of pores from 20 to 5 increases the discrepancy between the pore scale and volume average methods. Furthermore, for a cavity with a high Richardson number, where natural convection is dominant, a difference between the results of the two approaches is observed even for porous layer with 20 pores in vertical direction. This discrepancy is attributed to the influence of the transverse velocity component within the porous layer, which was neglected in this study.

*Corresponding Author
Email: moghtada.mobedi@shizuoka.ac.jp
Tel: +(81) 53 481 639

©2025 Tazawa *et al*. Published by Avanti Publishers. This is an open access article licensed under the terms of the Creative Commons Attribution Non-Commercial License which permits unrestricted, non-commercial use, distribution and reproduction in any medium, provided the work is properly cited. (http://creativecommons.org/licenses/by-nc/4.0/)

1. Introduction

Heat transfer in porous media is prevalent in numerous industrial and natural applications, leading to extensive research in this field. The studies have focused on conduction, convection, and/or radiation heat transfer through porous media. Research in this field is conducted both theoretically and experimentally. Analyzing heat transfer within a porous medium presents challenges due to the presence of two phases: solid and fluid. In certain scenarios, such as boiling within a porous medium, the phase number increases to three (solid, liquid, and vapor), further complicates the analysis [1, 2].

The most common theoretical study of heat transfer through a porous medium is computational study. Generally, two approaches exist for determining velocity, pressure, and temperature distributions in fluid-filled porous media: pore scale method (PSM) and volume average method (VAM). For pore scale method, the main governing equations are continuity, momentum and energy equations for the fluid flowing through the voids, while the heat conduction equation is solved for solid phase. This requires to define two regions in the computational solvers: voids and solid where heat transfer occurs at the interface between them. Mesh must be generated for both regions properly to provide the heat flow at the interface. Due to the pore scale irregular shapes of many porous media, generating a suitable mesh and solving the governing equations present challenges and demand considerable computational resources. Furthermore, the large number of pores (which are typically fine mesh) in a porous medium significantly increases the mesh number, demanding a significant amount of computing power and extended run time for accurate results. It must be mentioned that accurate velocity, pressure, and temperature results can be achieved if the governing equations are solved appropriately and the mesh resolution is sufficient for both the fluid and solid domains. Some computational pore scale studies which are reported in literature are Imani and Hooman [3] who studied natural convection in a differentially heated enclosure which is filled by bidisperse porous medium, Stockinger *et al*. [4] studied combustion process within the porous structure of soot filters by using lattice Boltzmann method, a study about the conjugate heat transfer simulations to explore the turbulent flow and heat transfer features in a composite porous-fluid system at the pore scale which was done by Alruwaili *et al*. [5], and the study of Celik *et al*. [6, 7] who performed two numerical works: one for determination of permeability and inertia coefficient and another study for determination of interfacial heat transfer and thermal dispersion of aluminum metal foam by using x-ray microtomography technique. Furthermore, Imani *et al* [8] studied unconsolidated porous media in a channel under forced convection, Wang *et al* [9] investigated the effect of unconsolidated and consolidated porous structures for thermoelectric cooler, Xuan *et al*. [10] did a numerical study in significance of the natural convection to the heat transfer of porous media by using pores media. The literature also contains other studies on the pore-scale analysis of heat and fluid flow in porous media [11-17].

As it was mentioned before, although the pore scale method yields accurate results for heat and fluid flow in porous media, its application is impractical and cumbersome when a porous medium contains many pores. Therefore, the volume average method is often preferred for solving most heat transfer problems in porous media. Defining the volume averaged quantity for a dependent variable such as φ is the first step of derivation of the volume averaged equations.

$$\langle\varphi\rangle = \varphi - \varphi' \tag{1}$$

where $\langle\varphi\rangle$ is the volume averaged quantity of φ over the representative control volume and φ' is the difference between the real value of φ and volume averaged value. Integrating of pore scale continuity, momentum and energy equations over a representative control volume (i.e., RCV) in the porous media, using definition given by Eq. (1) and applying necessary mathematical theorems in this field yield the volume average governing equations for VAM. Detailed information about the derivation of the volume average continuity, momentum and energy equations can be found in Ref. [18-20]. Fig. (**1**) compares the computational domain for PSM and VAM. Solid or fluid phase domains are not continuous for the entire real domain of the problem. If any line is plotted in the pore scale domain, the discontinuity of the solid and fluid phases can be observed.

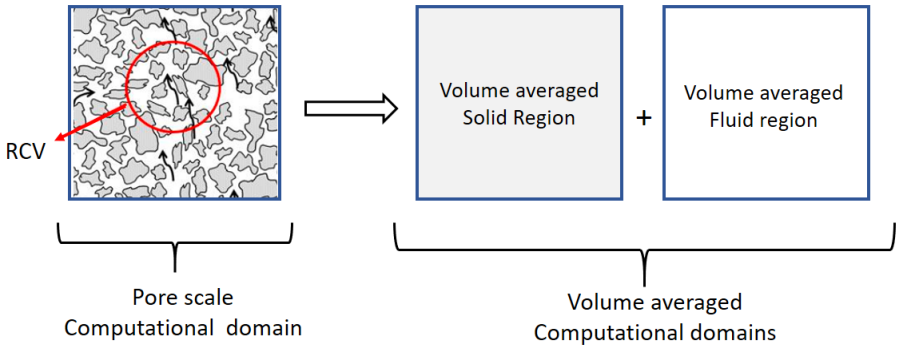

Figure 1: Comparison between pore scale and volume averaged computational domains.

However, there are two separate continuous domains for the VAM governing equations which are continuous domains for solid and fluid phases. These continuous domains allow the volume-averaged governing equations to be solved with fewer computational challenges.

To apply VAM approach, the values of some additional macroscopic transport parameters such as permeability, inertia coefficient, effective thermal conductivity, interfacial heat transfer coefficient between the phases as well as thermal dispersion are required. These volumetric transport parameters can be obtained experimentally or numerically. These transport parameters strongly depend on the porosity of the porous media, thermophysical properties of the solid and fluid phases, pore configuration and the characters of flow and heat through the porous media. The values of VAM transport parameters play an important role on the accuracy of the obtained results. Engineers and researchers should carefully evaluate VAM transport values when using the volume averaging method to ensure the accuracy of the obtained results. Some examples for the use of volume average method in a porous media are the study of Kiyak and Öztop [21] who used VAM continuity, momentum and energy equations for the porous structure in a cavity filled with PCM in order to enhance thermal energy storage, Astanina *et al*. [22] published a paper on the numerical study in a cavity filled with porous media and having a local heater on the floor to for a temperature dependence fluid, Izadi *et al* [23] performed a study on free convection of nanofluids in a cavity filled with porous media under time periodic heating and external magnetic field, Diganit *et al*. [24] and Jadhav *et al*. [25] published papers on the enhancement of heat transfer using discrete metal foam in a solar air heater by LTNE method and the use of functionally graded metal foams under partially filled condition in a heat exchanger. Moreover, Fteiti *et al*. [26] investigate the impact of random porosity distribution on the composite metal foam-phase change heat transfer, Aleshkova and Sheremet [27] have a study on the unsteady conjugate natural convection in a square enclosure filled with a porous medium and Öztop *et al*. [28] studied natural convection heat transfer in a partially opened cavity filled with porous media. The literature also contains other studies on the application of the volume averaging method to determine velocity, pressure, and temperature within the solid and fluid domains [29-35].

The comparison between pore-scale and volume-averaged methods has also attracted the attention of several researchers. For instance, Miansari *et al*. [36] conducted a numerical study to compare the pore scale and volume average approaches for natural convection in a cavity filled with unconsolidated particle placed randomly. Wang and Mobedi [37] performed a numerical study on the comparison of the pore scale and volume average analysis of the heat and fluid flow for a solid/liquid phase change in a 3D cubic Lattice Metal Frame (LMF). They also studied the effect of porosity and unit cell number on the applicability of the volume average approach in closed-cell porous media [38].

It is essential that sufficient number of particles or pores must exist within the porous domain for application of VAM. For example, VAM is not applicable to a porous medium with only two particles. This raises a question: what is the enough particles or pores for VAM application in a porous medium? This question motivated the present study, which focuses on the mixed convection heat transfer in a ventilated enclosure, differentially side-heated and partially filled with a vertical thin porous medium. The study examined various Richardson numbers and number of pores. The results obtained from the pore-scale method and the volume average method were

compared for the considered values of different governing parameter. The applications relevant to the present problem involve flow through metal woven wires to enhance heat transfer in channels and heat exchangers, the use of metal filters in wide-ranging applications such as pumps and valves, and thin porous membranes made of metals like palladium or ceramics for gas separation. To the authors' best knowledge, this is the first study to investigate the applicability of the volume average method for a thin porous layer, and the obtained results are expected to attract significant attention from researchers in this field.

2. Physical Model

The considered problems for the pore scale domain and volume average domain are shown in Fig. (**2**). It is an enclosure with the size of $L \times L$ and a part of the enclosure ($3L/10 \times L$) is filled with a thin porous medium with porosity 0.67. The top and bottom boundaries of the cavity are thermally insulated, and the left and right boundaries are maintained at different constant temperaturesT_H and T_C, respectively except the inlet and outlet regions with height of $L/5$. The inlet and outlet regions are located on the top of the right wall and the bottom of the left wall. The working fluid enters the enclosure from the inlet region with velocity of $-u_i$ and temperature of T_C, and then flows through the thin porous medium, then leaves the cavity from the outlet region on the bottom of the left wall. In the pore scale method, the number of pores changes from 5 to 20 by changing the number of the particles. For instance, a cavity may have a vertical porous layer with 5 pores and two particles in horizontal direction and six rectangular particles in vertical direction. Another important factor in the arrangement of particles within thin porous media is that the particles attached to the top and bottom walls have half height of the particles in the middle.

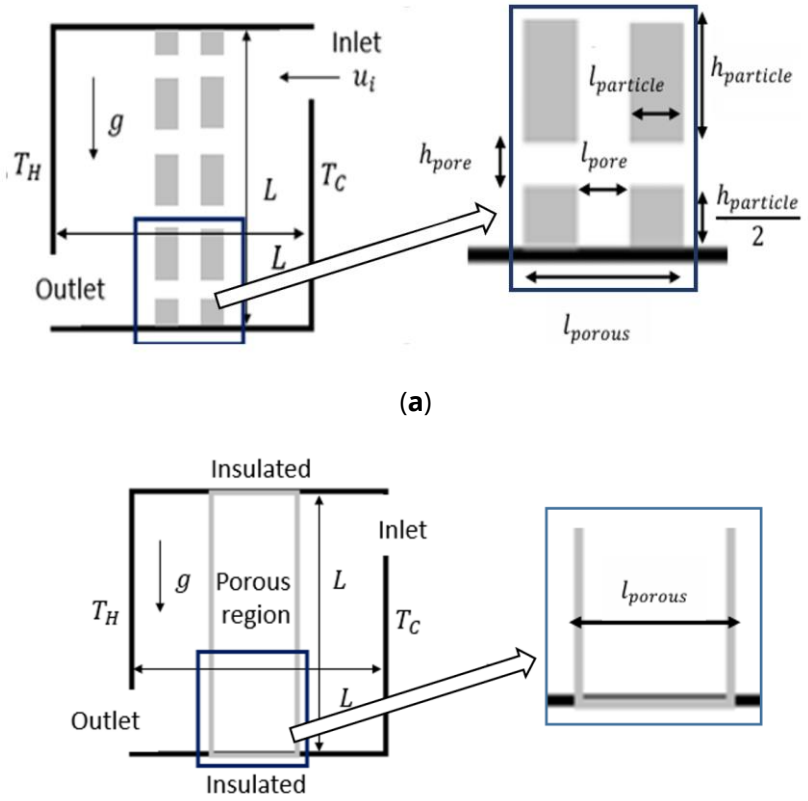

Figure 2: A schematic view of the computational domains **a**) pore scale domain, **b**) volume average domain.

Further details regarding particle and pore sizes are provided in Table **1**. In the volume average method, there are two regions as a region with clear fluid and a region with thin porous layer. Therefore, two different sets of governing equations must be solved simultaneously to determine the velocity, pressure, and temperature

throughout the entire cavity. It is assumed that there is no fluid flow in the vertical direction inside the thin porous region. All external geometries of the cavity and thin porous layer are the same for the domains of pore scale and volume average methods. The working fluid is air, and the material of the particles is aluminum.

Table 1: The geometrical details about structure of considered problem.

Parameter	Pore Scale			Volume Average
	5 Pores	10 Pores	20 Pores	
Length	L			
Height	L			
Total number of particles	12	22	42	-
Length of particle	L/10			-
Height of particle	L/10	L/20	L/40	-
Length of porous domain	3L/10			
Height of domain	L			
Inlet height	L/5			
Outlet height	L/5			

The thermophysical properties of air and aluminum used in this study are shown in Table **2**. The gravity affects in -y direction, and its contribution is included. The effect of radiation heat transfer is neglected. A local thermal equilibrium (LTE) between fluid and the porous medium is assumed in the volume average method. Several factors in this study suggest that the LTE assumption is reasonable. Firstly, the unconsolidated porous medium, composed of disconnected particles, provides a significantly large interfacial surface area that promotes heat transfer between the solid and fluid. Secondly, since the particles are only surrounded by the flowing fluid and are they not connected to a hot or cold surface, (also no heat generation), thermal exchange only occurs with the fluid. Thirdly, the steady-state conditions of our simulations allow sufficient time for this thermal exchange to bring the solid and fluid phases close to equilibrium, thus it can be assumed that a close coupling between temperatures of the solid and fluid phases exists.

Table 2: The thermophysical properties of considered parameters [39].

Parameter	Air	Aluminum
Density (kg/m^3)	1.166	2700
Specific heat capacity (J/kgK)	1006	900
Thermal conductivity (W/mK)	0.025	200
Dynamic viscosity (Pa·s)	1.8 x 10^{-5}	-
Prandtl number (-)	0.7	-

3. Governing Equations

The governing equations and boundary conditions for both cases of pore scale and volume average methods are presented separately in this section.

3.1. The Dimensional Form of Pore Scale Governing Equations

The dimensional governing equations, which are continuity, momentum and energy equations, are solved for pore scale problem.

$$\vec{\nabla} \cdot \vec{V} = 0 \tag{2}$$

$$(\vec{V} \cdot \vec{\nabla})\vec{V} = -\frac{1}{\rho_f}\vec{\nabla}p + \nu_f \vec{\nabla}^2 \vec{V} + g\beta(T - T_c)\vec{j} \tag{3}$$

$$(\rho C_p)_f \vec{V} \cdot \vec{\nabla} T_f = k_f \vec{\nabla}^2 T_f \ : \text{for fluid} \tag{4}$$

$$\vec{\nabla}^2 T_s = 0 : \text{for solid} \tag{5}$$

where β, C_p and k_f denote the thermal expansion coefficient, specific heat and thermal conductivity of air, respectively. T_f and T_s are fluid and solid temperatures.

3.2. The Dimensionless Form of Pore Scale Governing Equations

The dimensionless form of the above equations are obtained and written below:

$$\vec{\nabla}^* \cdot \vec{V}^* = 0 \tag{6}$$

$$(\vec{V}^* \cdot \vec{\nabla}^*)\vec{V}^* = -\vec{\nabla}^* p^* + \frac{1}{Re}\vec{\nabla}^{*2}\vec{V}^* + \frac{Gr}{Re^2}\theta_f \vec{j} \tag{7}$$

$$\vec{V}^* \cdot \vec{\nabla}^* \theta_f = \frac{1}{Re \cdot Pr}\vec{\nabla}^{*2}\theta_f \ : \text{for fluid} \tag{8}$$

$$\vec{\nabla}^{*2}\theta_s = 0 : \text{for solid} \tag{9}$$

where Re and Pr are Reynolds and Prandtl numbers. For the mixed convection heat transfer, there is also a dimensionless parameter as Gr/Re^2, known as Richardson number and it is shown by Ri. The following dimensionless parameters are used to obtain the dimensionless form of the PSM governing equations (Eqs. 6-9),

$$\vec{V}^* = \frac{\vec{V}}{u_i}\ ;\ \vec{\nabla}^* = \frac{\vec{\nabla}}{L}\ ;\ p^* = \frac{p}{\rho_f u_i^2}\ ;\ \theta = \frac{T - T_C}{T_H - T_C} \tag{10}$$

where L is the cavity height and u_i is the inlet velocity. θ also shows the dimensionless temperature. The dimensionless governing parameters are Grashof number (i.e., Gr), Reynolds number (i.e., Re), Prandtl number (i.e., Pr) and Richardson (i.e., Ri) defined as:

$$Gr = \frac{g\beta(T_H - T_C)L^3}{\nu_f^2}\ ;\ Re = \frac{u_i L}{\nu_f}\ ;\ Pr = \frac{\nu_f}{\alpha_f}\ ;\ Ri = \frac{Gr}{Re^2} \tag{11}$$

The Reynolds number at the inlet is 200, and as the flow expands within the cavity, the Reynolds number decreases. The Grashof number for the cavity without an inlet and outlet is 1.51×10^6, which is close to the critical Grashof number (10^6), indicating a laminar flow for pure natural convection heat transfer in the cavity.

3.3. The Dimensional Form of Volume Average Governing Equations

As it was mentioned before, the volume average method cavity consists of two regions as porous layer region and clear fluid region. The dimensional and dimensionless form of the governing equations for clear fluid region are the same with the fluid governing equations of the pore scale cavity (Eqs. 2-4) and Eqs. (6-8), respectively. Therefore, they are not written and discussed in this section. The focus of this sub-section is on the volume average governing equations for the thin porous layer. The volume average of a dependent quantity (such as φ) over a representative volume (i.e., REV) of the porous media can be defined as follows,

$$\langle \varphi \rangle = \frac{1}{V}\int_V \varphi \, dV \tag{12}$$

where V is the total volume of representative control volume. Similarly, intrinsic volume average for any dependent quantity (such as φ) of the porous medium is defined as.

$$\langle\varphi\rangle^x = \frac{1}{V^x}\int_{V^x} \varphi \, dV \tag{13}$$

where V^x is the volume of the considered phase (fluid or solid phase) in the REV. In this study, it is assumed that a local thermal equilibrium exists between the solid and fluid surrounds the solid.

$$\langle T\rangle^s \approx \langle T\rangle^f \approx \langle T\rangle \tag{14}$$

Therefore, there will be one energy equation represents both the temperature of the solid and fluid. Taking volume average from the pore scale equations (Eqs. 2- 5), using the definitions of Eqs. (12) and (13), and applying mathematical theorems in this field (as written by Ozgumus [20] for the energy equation), the volume averaged equations for fluid and solid can be obtained.

$$\vec{\nabla}\cdot\langle\vec{V}\rangle = 0 \tag{15}$$

$$\frac{1}{\varepsilon^2}\left(\langle\vec{V}\rangle\cdot\vec{\nabla}\right)\langle\vec{V}\rangle = -\frac{1}{\rho_f}\vec{\nabla}\langle p\rangle^f + \frac{\nu_f}{\varepsilon}\vec{\nabla}^2\langle\vec{V}\rangle - \frac{\nu_f}{K}\langle\vec{V}\rangle - \frac{C_F}{\sqrt{K}}\left|\langle\vec{V}\rangle\right|\langle\vec{V}\rangle + g\beta\left(T - T_{ref}\right)\vec{j} \tag{16}$$

$$\left(\rho C_p\right)_f\langle\vec{V}\rangle\cdot\vec{\nabla}\langle T\rangle = k_{eff}\vec{\nabla}^2\langle T\rangle \tag{17}$$

where $\langle\vec{V}\rangle$, $\langle p\rangle^f$ and $\langle T\rangle$ are the volume average velocity vector, intrinsic volume average pressure, and volume average temperature, respectively. ε, K, C_F and k_{eff} are porosity, permeability, inertia coefficient and effective thermal conductivity. As it was mentioned before, the porosity is fixed as 0.67 while the values of K, C_F and k_{eff} depends on the porous media structure and thermophysical properties of the solid and fluid, and that's why it must be calculated for each case.

3.4. The Dimensionless Form of Volume Average Governing Equations

The dimensionless form of volume average governing equations can be found by using the same dimensionless parameters presented by Eqs. (10) and (11).

$$\vec{\nabla}^*\cdot\langle\vec{V}^*\rangle = 0 \tag{18}$$

$$\begin{aligned}\frac{1}{\varepsilon^2}\left(\langle\vec{V}^*\rangle\cdot\vec{\nabla}^*\right)\langle\vec{V}^*\rangle = -\vec{\nabla}^*\langle p^*\rangle^f + \frac{1}{\varepsilon Re}{\vec{\nabla}^*}^2\langle\vec{V}^*\rangle - \frac{1}{Re\cdot Da}\langle\vec{V}^*\rangle \\ - \frac{C_F}{\sqrt{Da}}\left|\langle\vec{V}^*\rangle\right|\langle\vec{V}^*\rangle + \frac{Gr}{Re^2}\langle\theta\rangle\vec{j}\end{aligned} \tag{19}$$

$$\langle\vec{V}^*\rangle\cdot\vec{\nabla}^*\langle\theta\rangle = \frac{1}{Re\cdot Pr}{\vec{\nabla}^*}^2\langle\theta\rangle \tag{20}$$

where $\langle\vec{V}^*\rangle$, $\langle p^*\rangle^f$ and $\langle\theta\rangle$ are dimensionless volume average velocity vector, dimensionless intrinsic volume average pressure, and dimensionless volume average temperature, respectively. The definition of Reynolds and Prandtl numbers were given before by Eq. (11), however there is an additional dimensionless number in Eq. (19) called as Darcy number (i.e., Da). Darcy number is defined as:

$$Da = \frac{K}{L^2} \tag{21}$$

where K is permeability of the porous layer.

3.5. Boundary Conditions

The temperatures of the left and right walls are set to T_H and T_C, respectively (except inlet and outlet ports) and they are maintained at the same temperatures for the entire process. The top and bottom walls are insulated. Non-slip boundary conditions are applied for all walls. The fluid flow enters the domain from inlet part on the right wall and leaves the cavity from outlet part on the left wall. The dimensionless boundary conditions are given mathematically below:

Table 3: The employed boundary condition in this study.

		Pore Scale	Volume Average
Inlet	$x^* = 1$ $0.8 \le y^* \le 1$	$u^* = -1$ $v^* = 0$ $\theta_f = 0$	$\langle u^* \rangle = -1$ $\langle v^* \rangle = 0$ $\langle \theta \rangle = 0$
Outlet	$x^* = 0$ $0 \le y^* \le 0.2$	$\frac{\partial u^*}{\partial x^*} = \frac{\partial v^*}{\partial x^*} = \frac{\partial \theta_f}{\partial x^*} = 0$	$\frac{\partial \langle u^* \rangle}{\partial x^*} = \frac{\partial \langle v^* \rangle}{\partial x^*} = \frac{\partial \langle \theta \rangle}{\partial x^*} = 0$
Left wall	$x^* = 0$ $0.2 \le y^* \le 1$	$u^* = v^* = 0$ $\theta_f = 1$	$\langle u^* \rangle = \langle v^* \rangle = 0$ $\langle \theta \rangle = 1$
Right wall	$x^* = 1$ $0 \le y^* \le 0.8$	$u^* = v^* = 0$ $\theta_f = 0$	$\langle u^* \rangle = \langle v^* \rangle = 0$ $\langle \theta \rangle = 0$
Top and Bottom walls	$y^* = 0, 1$	$u^* = v^* = 0$ $\frac{\partial \theta_f}{\partial y^*} = 0$	$\langle u^* \rangle = \langle v^* \rangle = 0$ $\frac{\partial \langle \theta \rangle}{\partial y^*} = 0$

3.6. Solution Technique

In this study, OpenFOAM software is used to solve the governing equations of pore scale and volume average methods. The standard solver of OpenFOAM which is chtMultiRegionFoam is employed. It was used both for pore scale study and volume average cavity. A chtMultiRegionFoam solver is a transient solver for buoyant, laminar and turbulent flows and solid heat conduction as well as conjugate heat transfer of solid and fluid problems. Parallel processing was done by using 3 processors and the problem decomposed to 3 processors, and after finishing the runs, the results of 3 processors reconstructed and plotted. The absolute and relative tolerance for all dependent variables are 10^{-7} and 0.01. The relaxation factor for the momentum and energy equations are fixed as 0.5. Fig. (**3**) shows a sample of mesh for fluid region used in this study. A special attention was paid to have enough number of mesh between the particles in order to simulate the flow between the particles accurately. Number of mesh changed based on the number of particles in the thin porous layer. The number of mesh changes from 100000 to 160000 for the pore scale domain while for volume average domain these values changes 400000 and 640000.

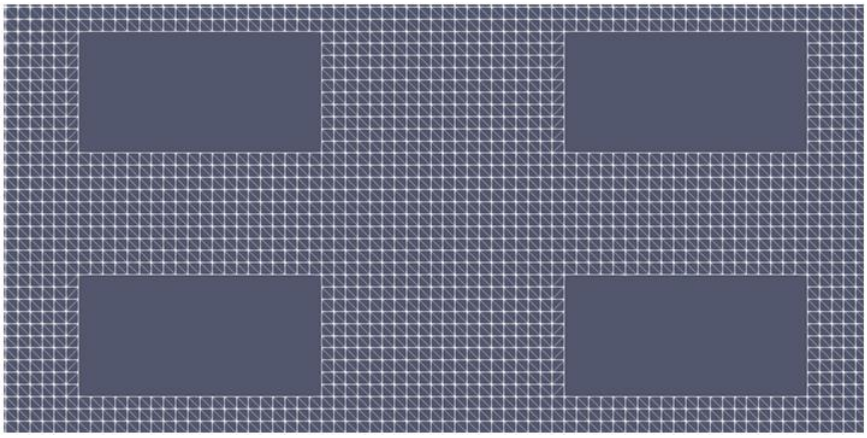

Figure 3: A schematic view of the mesh for the fluid region in the studied pore scale domain.

Mesh independency analysis was conducted to determine the appropriate number of mesh required to achieve accurate results. Fig. (**4**) presents a graph prepared to check the mesh number for the velocity and temperature results when Ri = 0, Re = 1000 and the number of particles in the vertical direction is 20. It shows the velocity profile in the gap between two neighboring particles in the vertical direction, at the center of the porous layer. Y axis is the distance in y direction while x axis is the velocity component in x direction. The number of mesh elements in the void between the particles was varied from 4 to 12, and it was observed that an almost identical velocity profile was obtained after using 10 mesh. In this study, the number of mesh between two particles changes based on the number of particles in vertical direction but the number of mesh was at least 10.

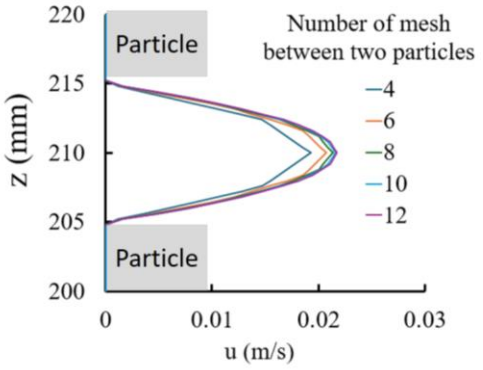

Figure 4: The velocity profiles in the gap between two particles for different mesh numbers when Ri = 0, Re = 1000 and the number of particles in the vertical direction is 20.

Furthermore, for the same cavity shown in Fig. (**4**), the average Nusselt number of the left wall (x = 0) was calculated for different numbers of mesh both for pore-scale (PSM) and volume-averaged (VAM) methods, and the results are presented in Table **4**. The average Nusselt number was calculated using the following equation:

$$\overline{\mathrm{Nu}} = \frac{\int_{X=l}^{X=H} -k\frac{dT}{dx}\Big|_{x=0} dy}{T_H - T_c} \tag{22}$$

The number of employed mesh number for VAM is 800 x 800 and for PSM is 400 X 400 in this study. Table **4** demonstrates that numbers of mesh used in this study are sufficient to obtain accurate results.

Table 4: Variation of the average Nusselt number of the left wall with the number of mesh for PSM and VAM methods at Ri = 0, Re = 1000, and for a case with 20 particles in the y-direction.

VAM			PSM		
Mesh Number	$\overline{\mathrm{Nu}}$	**Relative Error [%]**	**Mesh Number**	$\overline{\mathrm{Nu}}$	**Relative Error [%]**
100 x 100	18.21		160 x 160	17.67	
200 x 200	17.57	3.30	240 x 240	17.38	1.64
400 x 400	17.29	1.59	320 x 320	17.25	0.75
600 x 600	17.04	1.45	400 x 400	17.20	0.29
800 x 800	17.01	0.21	480 x 480	17.20	0.00

For Ri = 1.0, Re =1000 and 20 pores in transverse direction, the longitudinal air velocity between two pores is 0.016 m/s, and the particle length is 40 mm. Assuming no neighboring particle influence, the calculated boundary layer thickness at the end of the horizontal particle is 30.8 mm. In this study, the mesh size near the particle in the transverse direction is 1 mm, which is sufficient to resolve the boundary layer. Furthermore, the performed mesh independency study demonstrates that the employed mesh between the particles is sufficiently fine to yield accurate results.

All simulations were performed on a personal computer in our laboratory equipped with an Intel Core i7-9700 CPU @ 3.00GHz and 80GB of RAM. The wall-clock run time was observed to depend on the number of pores in the vertical porous layer as well as the Richardson number. For example, solving a case with Ri = 0, Re = 1000 and 20 pores in the vertical direction took 85255 seconds for the pore scale approach, while for the volume average approach required 69768 seconds. As it was mentioned before, the aim of this study is to determine the minimum number of pores in the y-direction required to obtain acceptable results from the VAM. However, it's important to note that in practical applications, the number of pores in the y-direction can be considerably higher than 20, and pore-scale simulations must be done with much more number of mesh and it will take significantly longer time compared to the volume-averaged method.

4. Results and Discussion

The obtained results of this study are discussed in two sub-section: a) determination of porous media transport parameters, b) comparison of the pore scale and volume average results.

4.1. Determination of Porous Media Transport Parameters

As it can be seen from the Eqs. (15-17), the values of volume averaged transport parameters which are permeability, inertia coefficient, and effective thermal conductivity are needed to obtain volume average results. It must be mentioned that the value of thermal dispersion is also needed but the effect of thermal dispersion is ignored since the porous layer is thin.

4.1.1. Determination of Permeability and Inertia Coefficient

Permeability and inertia coefficient depend on the structure of porous media, even small changes in a structure may change the values of permeability and inertial coefficient considerably. In addition to experimental methods, some theoretical methods are also suggested in literature to determine the permeability and inertia coefficient of a porous medium [40-44]. The method that is used in this study is explained in this section. The structure of thin porous media changes by changing number of block rows. Therefore, for each number of particles in vertical direction, permeability and inertia coefficient are calculated. To determine the value of permeability and inertia coefficient, fluid flow in a representative domain is considered as shown in Fig. (**5a**). Top and bottom surfaces are symmetry. The channel has three regions as inlet, representative domain and outlet regions. The representative domain contains 4 solid particles. Fluid enters the channel with an inlet velocity of u_i. The value of u_i calculated based on the considered Reynolds number. It must be mentioned that pore scale Reynolds number is calculated based on the height of representative control volume which is h. The pore scale governing equations (Eqs. (2-5)) are solved for the channel of Fig. (**5a**) and the velocity and pressure drop distributions are obtained. The pressure in the inlet side is high and it is low in the outlet side as shown in Fig. (**5b**). There is a pressure drop between the particles of the inlet and outlet sides (i.e., flow direction), however there is no pressure change in y direction since both top and bottom sides are symmetry.

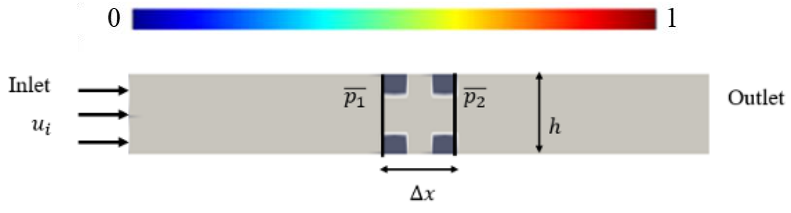

(**a**)

(**b**)

Figure 5: Domain for determination of permeability and inertia coefficient when Re = 17, **a**) considered domain, **b**) pressure distribution.

If the volume average flow is considered, the flow is one dimensional, means that $\langle v \rangle$ velocity component is zero and the volume average pressure drop in y direction does not exists. Therefore, Eq. (16) can be reduced to the following form,

$$-\frac{d\langle p \rangle}{dx} = \frac{\mu}{K}\langle u \rangle + \frac{C_F}{\sqrt{K}}\rho_f |\langle u \rangle| \langle u \rangle \tag{22}$$

This equation in the dimensionless form can be rewritten as:

$$\Pi = A + BRe \tag{23}$$

where the dimensionless parameters of Π, A and B are defined as:

$$\Pi = -\frac{h^2}{\mu\langle u \rangle}\frac{d\langle p \rangle}{dx}, A = \frac{h^2}{K}, B = \frac{C_F h}{\sqrt{K}} \tag{24}$$

where h is the channel height. Based on the obtained pore scale velocity and pressure drop in the channel, the volume averaged velocity (which does not change through the channel) and the change of pressure drop between the inlet and outlet of the channel are obtained. After that, the dimensionless pressure drop (i.e., Π) can be calculated and plotted respect to Reynolds number as shown in Fig. (**6**). For the low Reynolds number range ($Re \leq$ 100), the dimensionless pressure drop is almost constant, while for high Reynolds number range ($Re \geq 100$), the pressure drop increases linearly with Reynolds number due to effect of inertia coefficient.

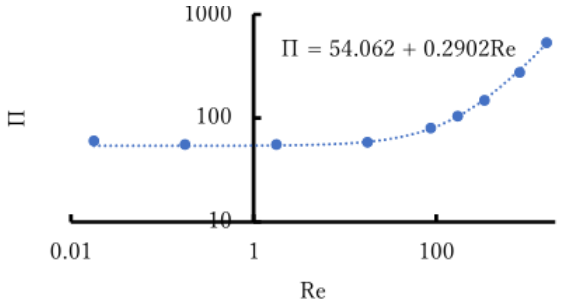

Figure 6: The change of dimensionless pressure drop with Reynolds number.

Finally, the permeability and inertia coefficient can be found by applying a curve fitting method. After determination of values of A and B, the obtained permeability and inertia coefficient of the porous media can be found by using Eqs. (24). For 3 row numbers (N = 5, 10 and 20), the permeability and inertia coefficient were calculated and presented in Table **5**.

Table 5: Permeability and inertia coefficient for three structures.

	$N = 5$	$N = 10$	$N = 20$
K [m^2]	7.60×10^{-6}	7.78×10^{-6}	8.39×10^{-6}
C_F [-]	0.0395	0.0146	0.00918

4.1.2. Effective Thermal Conductivity

The value of effective thermal conductivity is also required to solve the volume averaged governing equations (Eqs. (17)). In general, the thermal conductivity of a material can be obtained from the physical property's tables, however the effective thermal conductivity of porous media requires additional calculation. Effective thermal conductivity of a porous medium can be found experimentally or theoretically such as using Fourier law or other innovative methods suggested in literature [45-50]. In this section, the method used to determine effective thermal conductivity of porous layer is explained. Fig. (**7**) shows the representative cell of a considered problem to

find effective thermal conductivity and temperature distribution. The boundary condition of the left and right surfaces of the cell are constant temperature of T_H and T_C, respectively, while for the top and bottom surfaces are insulated. As it can be seen from Fig. (**7**), the temperature distribution is perpendicular to the heat transfer direction since the problem of one dimensional pure heat conduction.

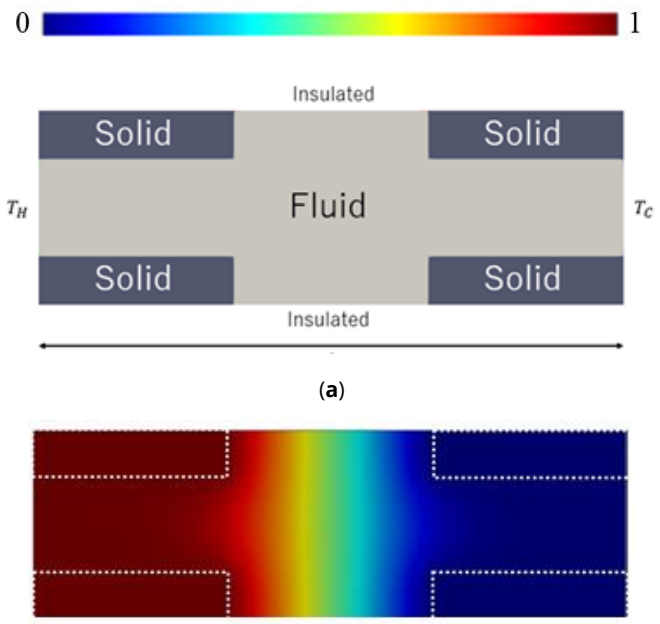

(**a**)

(**b**)

Figure 7: Determination of effective thermal conductivity, **a**) the considered representative volume, **b**) temperature distribution.

The effective thermal conductivity of the problem can be obtained by the following equations and the values are shown in Table **6**.

$$k_{eff} = \frac{q"l}{T_H - T_C} \tag{25}$$

where $q"$ represents heat flux calculated from the results and l is the distance between the two left and right surfaces.

Table 6: Effective thermal conductivity for different structure.

	$N = 5$	$N = 10$	$N = 20$
k_{eff} (W/m.k)	0.068	0.072	0.072

4.2. Comparison of PSM and VAM Results

4.2.1. Results for Low Values of Richardson Number (Ri = 0)

Fig. (**8**) shows the distribution of pore scale and volume average velocities magnitude and temperature for the different porous layers as N = 5, 10 and 20 when $Ri = 0$ and $Re = 1000$. The first two rows compare the magnitude of the velocity between the pore scale and volume average while the third and fourth rows compare the temperature distributions between the pore scale and volume average results.

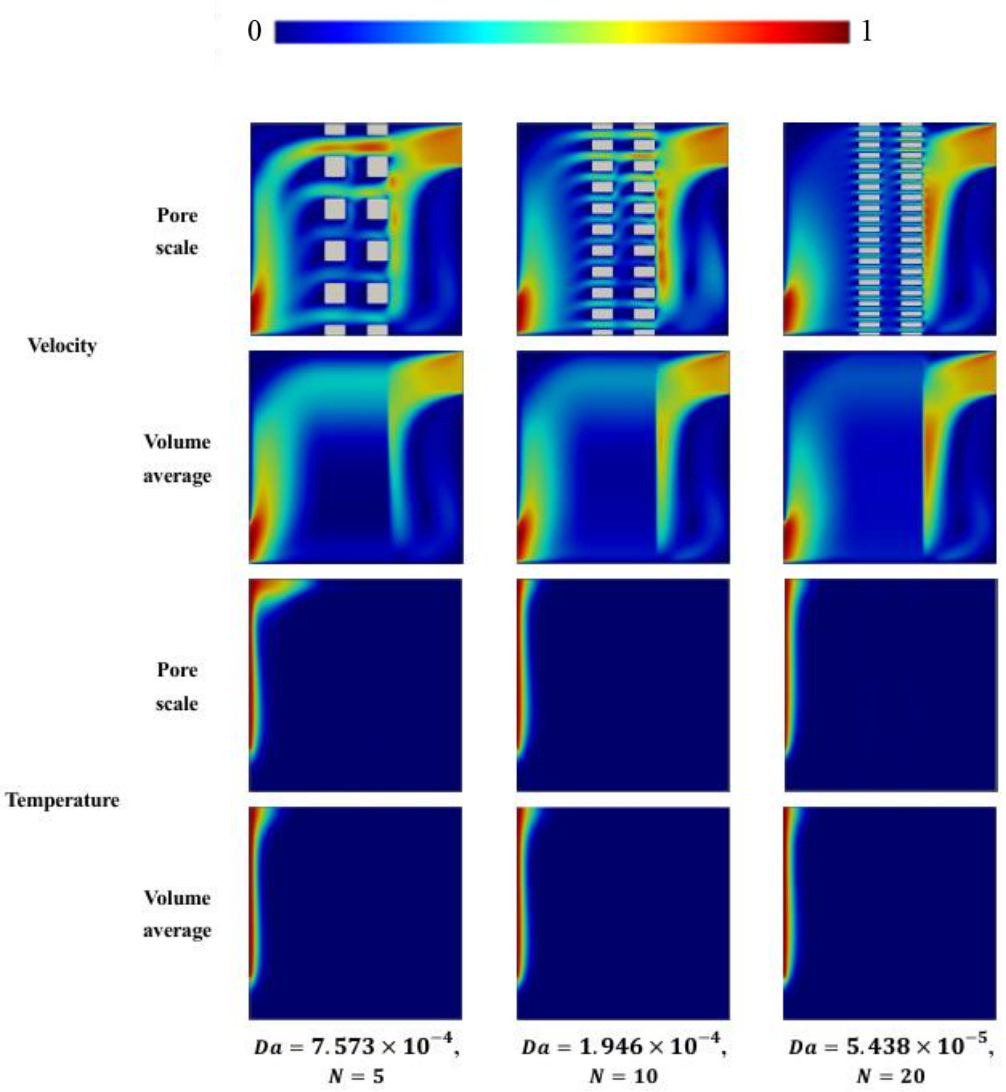

Figure 8: Pore scale and volume average velocity and temperature distributions in the ventilated enclosure when Ri = 0 and Re = 1000.

For the pore scale and volume average methods, the fluid comes from the inlet, flows through the porous region, distributed to each pore, moves toward left wall and finally exits from the outlet. For 5 pores structure, the largest velocity between the pores can be seen in the top pores since the forced convection is dominant and the most part of fluid from the inlet flows straightly toward porous media. As the Darcy number decreases (i.e., pore density increases vertically), the velocity magnitude becomes more uniform across the pores between the blocks. Comparison the results of the pore scale method and volume average method shows that the velocity distributions in the right and left regions of the porous layer get closer to each other by decreasing Darcy number. On the other hand, there is no temperature change in entire cavity and no big differences between the pore scale and volume average methods for the temperature distributions except for the structure with 5 pores in y^* direction for which a small change can be seen near the top of the left wall.

Fig. (**9**) shows the comparisons of the pore scale and volume average velocity magnitude and dimensionless temperature profiles of a vertical line (x^* = 0.8) in the right region and a vertical line (x^* = 0.2) in the left region. The first two rows show the comparison of magnitude of velocity for the left and right vertical lines while the third line shows the comparison of temperature. The temperature distribution for the right vertical comparison line is not plotted since no difference between the volume average and pore scale temperature profiles is observed. The results of velocities for PSM and VAM are close to each other for the vertical line in the right region. The differences between the results of two methods become smaller by increasing number of pores in vertical

direction. For the velocities on the left line (x^* = 0.2), the situation is different. A considerable difference is observed between the PSM and VAM for the structure of N = 5. However by increasing number of pores in vertical direction, the results between PSM and VAM gets closer to each other and for the structure with N = 20, a nice agreement can be seen. In other words, reducing Darcy number from $Da = 5.438 \times 10^{-5}$ (i.e. N= 5) to $Da = 1.946 \times 10^{-4}$ (i.e., N = 20) decreases the difference between PSM and VAM. As it was mentioned before, the temperature profile of pore scale method for N = 5 is different from that of volume average method on the top side. From Fig. (**9**), it can be concluded that after 10 number of pores in vertical direction the results of PSM and VAM are close to each other, however before N = 10 the attention about the accuracy of the results of VAM is required.

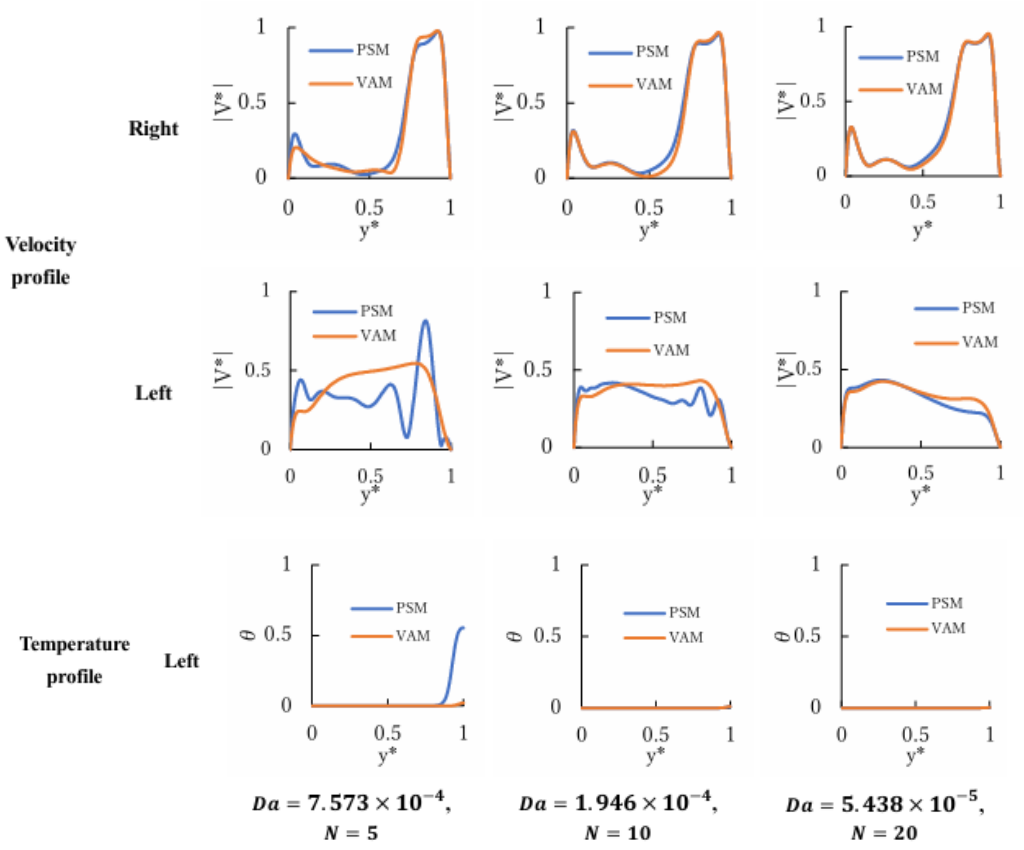

Figure 9: Pore scale and volume average velocity magnitude and temperature profiles when $Ri = 0$ and $Re = 1000$.

To have a value represents the difference between the results of pore scale and volume average methods, the absolute difference ratio of the dimensionless velocity magnitude and dimensionless temperature for the left and right lines (x^* = 0.2 and 0.8, respectively) are calculated by following equation.

$$e_\phi = \frac{\int_0^1 |\phi_{PSM} - \phi_{VAM}| dy^*}{\int_0^1 |\phi_{PSM}| dy^*} \times 100 \tag{26}$$

where ϕ is a dependent variable which can be $|V^*|$ or θ. e_ϕ shows the error between the results of two methods. The integral of these values are numerically calculated along the left and right lines (x^* = 0.2 and 0.8). The values of e_ϕ for the case of Re = 1000 and Ri = 0 for three studied structures are given in Table **7**. As observed, the total absolute difference ratio (e_ϕ) decreases with a reduction in the Darcy number (or an increase in vertical pore density). This indicates that the discrepancy between pore-scale and volume-averaged values diminishes as the vertical pore density increase. Thus, the applicability of volume average method increases for a thin porous layer when the Darcy number is sufficiently low. A minimum sufficient number of pores in vertical direction may be N = 10 since the average error is blow 20%.

Table 7: Absolute Difference Ratio when $Ri = 0$ and $Re = 1000$.

		$Da = 7.573 \times 10^{-4}$ $N = 5$	$Da = 1.946 \times 10^{-4}$ $N = 10$	$Da = 5.438 \times 10^{-5}$ $N = 20$
$e_{\lvert V^* \rvert}$	Right	10.9	7.9	2.3
	Left	45.3	19.8	9.7
e_θ	Left	98.0	23.8	11.8
Average	----	51.4	17.1	7.9

4.2.2. Results for High Values of Richardson Number (Ri = 7)

Fig. (**10**) shows the distribution of pore scale and volume average velocity and temperature for the different Darcy numbers when the $Ri = 7$ and $Re = 1000$. Similar to Fig. (**9**), the first two rows compare the velocity magnitude between the pore scale and volume average while the third and fourth rows compare the temperature distribution between two approaches. As it can be seen, in this case, natural convection is dominant, as a result the inlet flow in the right region goes down further and fluid flows in the bottom of the enclosure from the right to the left. For the pore scale velocity distribution of N = 5, the magnitude of velocity in y^* direction inside the porous region increases since the natural convection is dominant. The comparison between the temperature distributions of pore scale and volume average results shows that a difference exists for all three Darcy numbers even for the smallest Darcy number which a thin porous layer with 20 pores. The difference between these two methods across the three cases may be attributed to the vertical flow in the porous structure caused by natural convection.

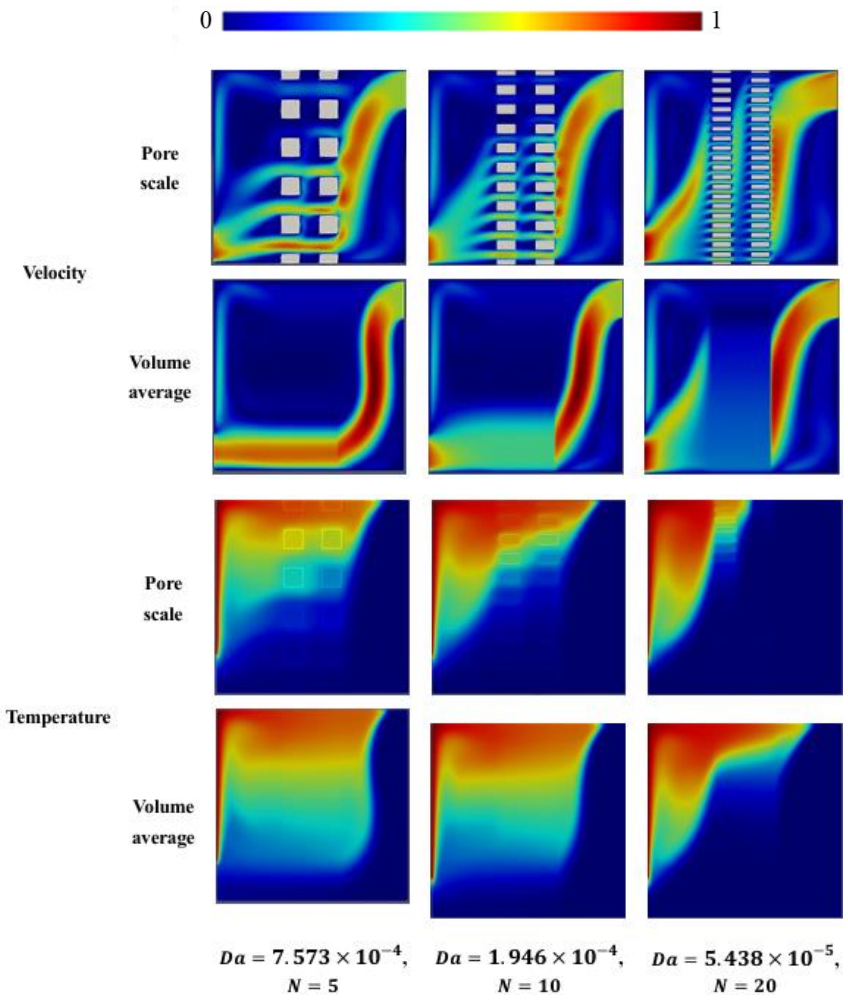

Figure 10: Pore scale and volume average velocity and temperature distributions when $Ri = 7$ and $Re = 1000$.

Fig. (**11**) shows comparisons of the pore scale and volume average velocity and temperature profiles for the right vertical line (x^*= 0.8) and left vertical line (x^*= 0.2). Significant discrepancies exist between the pore-scale and volume-averaged velocity profiles at both the right and left lines. This difference becomes smaller by reducing Darcy number. A linear temperature change can be seen for N = 5 and 10, while for N = 20, the temperature decreases in the top region. The temperature profiles demonstrate a trend of convergence between the pore-scale and volume-averaged methods as the vertical pore density increases.

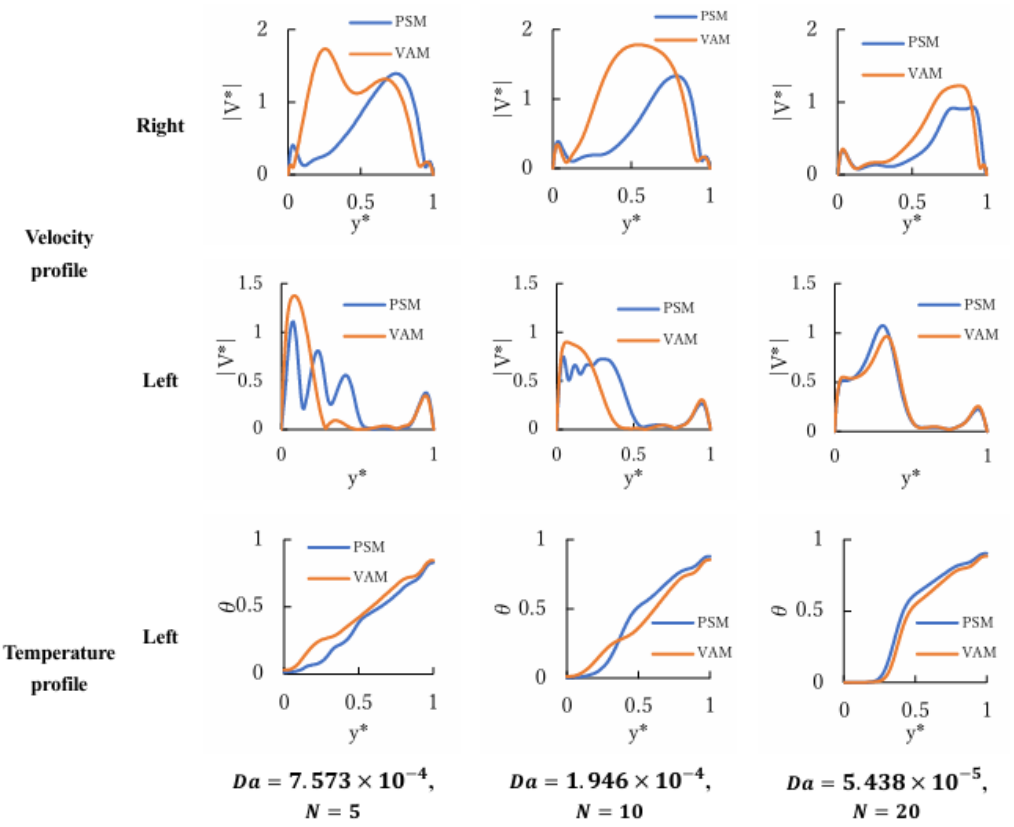

Figure 11: Pore scale and volume average velocity and temperature profiles when $Ri = 7$ and $Re = 1000$.

Table **8** shows the absolute difference ratio of magnitude of velocity and dimensionless temperature which is defined by Eq. (26). The values of e_ϕ are relatively higher compared to the case of other Richardson numbers which is $Ri = 0$. The reason for the high values of e_ϕ can be explained by the effect of natural convection. By increasing of Richardson number, the effect of the natural convection heat transfer increases and the role for the permeability and heat transfer in transverse direction becomes significant. As it was mentioned before, the transverse permeability and effective thermal conductivity are neglected in this study since the porous layer is thin. The present study shows that by increasing of Richardson number, the role of transverse flow on heat and fluid in the thin porous layer increases and this effect must be considered. No doubt that, by including transverse permeability and transverse effective thermal conductivity into the calculation, the results of pore scale and volume average methods will be closer to each other and the value of e_ϕ will decrease.

Table 8: The absolute difference ratio when $Ri = 7$ and $Re = 1000$.

		$Da = 7.573 \times 10^{-4}$ $N = 5$	$Da = 1.946 \times 10^{-4}$ $N = 10$	$Da = 5.438 \times 10^{-5}$ $N = 20$
$e_{\lvert V^* \rvert}$	Right	78.2	101.4	50.7
	Left	72.0	45.1	10.4
e_θ	Left	18.7	16.2	9.1
Average		56.3	54.3	23.4

5. Conclusions

In this study, heat and fluid flow in a ventilated enclosure with a thin porous medium is investigated numerically. The thin porous layer is located at the middle of the cavity and it separates the cavity into two equal parts. For the pore scale approach, the governing equations which are continuity, momentum and energy equations for fluid and heat conduction equations for the solid are solved, and pore scale velocity, pressure and temperature distributions for entire domain are obtained. For the volume average method, additionally, the volume average continuity, momentum and energy equations including porous media transport parameters such as permeability and effective thermal conductivity are solved. The results of this solution are volume average velocity, pressure and temperature for the porous structure. However, for the region without porous structure the pore scale governing equations are solved. After finding solution for both methods, the results of pore scale method and volume average method are compared. Following main remarks can be concluded,

a) When the Reynolds number is high and Richardson number is low (such as Re = 1000 and Ri = 0) the fluid flow in the cavity is affected by the vertical porous layer. The effect of porous layer is small for the porous layer with 5 pores (high permeability) while it is significant for the porous layer with 20 pores (low permeability).

b) For the case of Re = 1000 and Ri = 0, an excellent agreement between the results of pore scale and volume average is observed for porous layer with 20 pores. However, the agreement between two results decreases by decreasing number of pores in the porous layer. It seems that for the porous layer with 10 pores, almost accurate results by volume average can be obtained since the average of error is 17.1%.

c) For the high Reynolds and Richardson number (such as Re = 1000 and Ri = 7), the effect of the buoyancy increases. After entering of fluid into the cavity, it goes down and fluid passes the porous layer at the bottom of the cavity since right wall is cold. This is the reverse of flow observed for Re = 1000 and Ri =0.

d) The difference between the pore scale and volume average methods when Ri = 7 and Re = 1000 is considerably higher than the case with Ri = 0. The main reason is the assumption considered at the beginning of study which is negligible transverse permeability and effective thermal conductivity. Natural convection in the porous layer plays an important role in fluid flow through the porous structure, and transverse permeability and effective thermal conductivity must be considered for achieving accurate results from the volume average method.

Further investigations could extend this comparative study by considering different porosities as well as variations in the thermal properties of the solid and fluid phases. Therefore, a wider range of governing dimensionless numbers, such as the thermal conductivity ratio and porosity, will be taken into account to expand the validity study of the volume average method.

Conflict of Interest

The authors declare that no known competing financial interests or personal relationships influenced, or could have appeared to influence, the work reported in this paper.

Funding

No fund was used.

Nomenclature

A	=	Heat transfer area (m^2)
C_p	=	Specific heat (J/kgK)
C_F	=	Inertia coefficient
Da	=	Darcy number

e	=	Total absolute difference ratio
g	=	Gravity (m/s^2)
Gr	=	Grashof number
h	=	Height | Heat transfer coefficient (m | W/m^{2}K)
K	=	Permeability (m^2)
k	=	Thermal conductivity (W/mK)
L	=	Length of enclosure (m)
l	=	Length (m)
N	=	Number of pores
Nu	=	Nusselt number
p	=	Pressure (N/m^2)
Pr	=	Prandtl number
$q"$	=	Heat flux (W/m^2)
Re	=	Reynolds number
Ri	=	Richardson number
T	=	Temperature (K)
u	=	Velocity component in x direction (m/s)
v	=	Velocity component in y direction (m/s)
V	=	Velocity | Volume (m/s | m^3)
x, y	=	Cartesian coordinates (m)

Subscript and Superscript

C	=	Cold
eff	=	Effective
f	=	Fluid
H	=	Hot
i	=	Inlet
int	=	Interfacial
ref	=	Reference
s	=	Solid
$*$	=	Dimensionless symbol

Greek Symbols

α	=	Thermal diffusivity (m^2/s)
β	=	Volumetric expansion coefficient (1/K)
θ	=	Dimensionless temperature
μ	=	Dynamic viscosity (Pa·s)
ν	=	Kinematic viscosity (m^2/s)
Π	=	Dimensionless pressure drop
ρ	=	Density (kg/m^3)

References

[1] Mahmoudi Y, Hooman K, Vafai K. Convective heat transfer in porous media, CRC Press; 2019.

[2] Mobedi M, Hooman K. Advances of heat transfer in porous media, MDPI-Multidisciplinary Digital Publishing Institute; 2023. https://doi.org/10.3390/books978-3-0365-6711-2

[3] Imani G, Hooman K. Lattice Boltzmann pore scale simulation of natural convection in a differentially heated enclosure filled with a detached or attached bidisperse porous medium. Transp Porous Med. 2017; 116: 91-113. https://doi.org/10.1007/s11242-016-0766-z

[4] Stockinger C, Raiolo A, Alamian R, Hadjadj A, Nieken U, Shadloo MS. Lattice Boltzmann simulations of heterogeneous combustion reactions for application in porous media. Eng Anal Bound Elem. 2024; 166: 105817. https://doi.org/10.1016/j.enganabound.2024.105817

[5] Alruwaili W, Jadidi M, Keshmiri A, Mahmoudi Y. Pore-scale conjugate heat transfer analysis of turbulent flow over stochastic open-cell metal foams. Int J Thermal Sci. 2024; 202: 109061. https://doi.org/10.1016/j.ijthermalsci.2024.109061

[6] Celik H, Mobedi M, Nakayama A, Ozkol U. A numerical study on determination of volume averaged thermal transport properties of metal foam structures using X-ray microtomography technique. Numer Heat Transf Part A Appl. 2018; 74(7): 1368-86. https://doi.org/10.1080/10407782.2018.1494936

[7] Celik H, Mobedi M, Nakayama A, Ozkol U. A study on numerical determination of permeability and inertia coefficient of aluminum foam using x-ray micro tomography technique: focus on inspection methods for reliability (permeability and inertia coefficient by tomography). J Porous Media. 2019; 22(5): 511-29. https://doi.org/10.1615/JPorMedia.2019028887

[8] Imani G, Maerefat M, Hooman K. Pore-scale numerical experiment on the effectof the pertinent parameters on heat flux splitting at the boundary of a porous medium. Transp Porous Media. 2013; 98: 631-49. https://doi.org/10.1007/s11242-013-0164-8

[9] Wang C, Mobedi M, Yang X, Shen Y, Zhao H, Chen H, *et al*. A comparison study of heat dissipation module between the consolidated and unconsolidated porous structures for thermoelectric cooler, Appl Therm Eng, 2024; 247: 123085. https://doi.org/10.1016/j.applthermaleng.2024.123085

[10] Xuan ZH, Fang WZ, Lu YH, Yang C, Tao WQ. Significance of the natural convection to the heat transfer of porous media: A pore-scale study. Int J Heat Mass Transfer. 2024; 222: 125163. https://doi.org/10.1016/j.ijheatmasstransfer.2023.125163

[11] Wang C, Sugiura T, Mobedi M, Chen H. Comparison of heat transfer enhancement between open and closed cell porous metal structures for solid–liquid phase change. Int J Numer Methods Heat Fluid Flow. 2023; 33: 1797-1817. https://doi.org/10.1108/HFF-09-2022-0504

[12] Torabi M, Peterson GP, Torabi M, Karimi N. A thermodynamic analysis of forced convection through porous media using pore scale modeling. Int J Heat Mass Transfer. 2016; 99: 303-16. http://dx.doi.org/10.1016/j.ijheatmasstransfer.2016.03.127

[13] Jadidi M, Revell A, Mahmoudi Y. Pore-scale large eddy simulation of turbulent flow and heat transfer over porous media. Appl Therm Eng. 2022; 215: 118916. https://doi.org/10.1016/j.applthermaleng.2022.118916

[14] Hosseinalipour SM, Namazi M. Pore-scale numerical study of flow and conduction heat transfer in fibrous porous media. J Mech Sci Technol. 2019; 33: 2307-17. https://doi.org/10.1007/s12206-018-1231-4

[15] Tran Ngoc TD, Le NHN, Tran TV, Ahmadi A, Bertin H. Homogenization of solute transport in unsaturated double-porosity media: model and numerical validation. Transp Porous Media. 2020; 132: 53-81. https://doi.org/10.1007/s11242-020-01380-6

[16] Xiao T, Du Z, Song X, Peng W, Yang X, Sunden B. Effect of natural convection on charging of phase change materials in graded metal foam: Pore-scale simulation. Int Commun Heat Mass Transf. 2023; 149: 107080. https://doi.org/10.1016/j.icheatmasstransfer.2023.107080

[17] Sadeghi MA, Agnaou M, Barralet J, Gostick J. Dispersion modeling in pore networks: A comparison of common pore-scale models and alternative approaches. J Contam Hydrol. 2020; 228: 103578. https://doi.org/10.1016/j.jconhyd.2019.103578

[18] Whitaker S. The method of volume averaging (theory and applications of transport in porous media), Springer; 1999.

[19] Vafai K, Ed. Handbook of Porous Media. CRC Press; 2005.

[20] Ozgumus T. An experimental and numerical study on effects of pore to throat size ratio on macroscopic transport parameters in porous media, PhD thesis. Izmir Institute of Technology; 2015.

[21] Kıyak B, Öztop HF. Optimizing of partial porous structure for efficient heat transfer and thermal energy storage of phase change material in a rectangular cavity. J Therm Anal Calorim. 2024; 149: 13425-41. https://doi.org/10.1007/s10973-024-13634-2

[22] Astanina MS, Buonomo B, Manca O, Sheremet MA. Three-dimensional natural convection of fluid with temperature-dependent viscosity within a porous cube having local heater. Int Commun Heat Mass Transf. 2022; 139: 106510. https://doi.org/10.1016/j.icheatmasstransfer.2022.106510

[23] Izadi M, Alshuraiaan B, Hajjar A, Sheremet MA, Ben Hamida MB. Free convection of nanofluids in a porous sensible heat storage unit: Combined effect of time periodic heating and external magnetic field. Int J Therm Sci. 2023; 192: 108404. https://doi.org/10.1016/j.ijthermalsci.2023.108404

[24] Diganjit R, Gnanasekaran N, Mobedi M. Numerical study for enhancement of heat transfer using discrete metal foam with varying thickness and porosity in solar air heater by LTNE method. Energies. 2022; 15: 8952. https://doi.org/10.3390/en15238952

[25] Jadhav PH, Gnanasekaran N, Mobedi M. Analysis of functionally graded metal foams for the accomplishment of heat transfer enhancement under partially filled condition in a heat exchanger. Energy. 2023; 263: 125691. https://doi.org/10.1016/j.energy.2022.125691

[26] Miansari M, Gorji M, Ganji DD, Hooman K. Comparison between continuum and porous continuum models in studying natural convection in porous cavity with random distribution of solid obstacles. Int J Numer Methods Heat Fluid Flow. 2015; 25(3): 484-503. https://doi.org/10.1108/HFF-04-2014-0100

[27] Wang C, Mobedi M. A comprehensive pore scale and volume average study on solid/liquid phase change in a porous medium. Int J Heat Mass Transf. 2020; 159: 120102. https://doi.org/10.1016/j.ijheatmasstransfer.2020.120102

[28] Wang C, Zheng X, Zhang T, Chen H, Mobedi M. The effect of porosity and number of unit cell on applicability of volume average approach in closed cell porous media. Int J Numer Methods Heat Fluid Flow. 2021; 32(8): 2778-98. https://doi.org/10.1108/HFF-08-2021-0527

[29] Fteiti M, Ghalambaz M, Sheremet M, Ghalambaz M. The impact of random porosity distribution on the composite metal foam-phase change heat transfer for thermal energy storage. J Energy Storage. 2023; 60: 106586. https://doi.org/10.1016/j.est.2022.106586

[30] Aleshkova IA, Sheremet MA. Unsteady conjugate natural convection in a square enclosure filled with a porous medium. Int J Heat Mass Transf. 2010; 53: 5308-20. https://doi.org/10.1016/j.ijheatmasstransfer.2010.07.025

[31] Oztop HF, Al-Salem K, Varol Y, Pop I. Natural convection heat transfer in a partially opened cavity filled with porous media. Int J Heat Mass Transf. 2011; 54: 2253-61. https://doi.org/10.1016/j.ijheatmasstransfer.2011.02.040

[32] Peng C, Ming T, Tao Y. Thermal and hydraulic performances of a tube filled with various thermal conductivities of porous media. Int J Heat Mass Transf. 2015; 81: 784-96. http://dx.doi.org/10.1016/j.ijheatmasstransfer.2014.10.073

[33] Oztop HF. Natural convection in partially cooled and inclined porous rectangular enclosures. Int J Therm Sci. 2007; 46: 149-56. https://doi.org/10.1016/j.ijthermalsci.2006.04.009

[34] Yang X, Yu J, Guo Z, Jin L, He Y. Role of porous metal foam on the heat transfer enhancement for a thermal energy storage tube. Appl Energy. 2019; 239: 142-56. https://doi.org/10.1016/j.apenergy.2019.01.075

[35] Yang X, Wei P, Wang X, He Y. Gradient design of pore parameters on the melting process in a thermal energy storage unit filled with open-cell metal foam. Appl Energy. 2020; 268: 115019. https://doi.org/10.1016/j.apenergy.2020.115019

[36] Abu-Hamdeh NH, Oztop HF, Alnefaie KA. A computational study on mixed convection in a porous media filled and partially heated lid-driven cavity with an open side. Alexandria Eng J. 2020; 59: 1735-50. https://doi.org/10.1016/j.aej.2020.04.039

[37] Sheremet MA, Oztop HF. Impact of porous complicated fin and sinusoidal-heated wall on thermogravitational convection of different nanofluids in a square domain. Int J Therm Sci. 2021; 168: 107053. https://doi.org/10.1016/j.ijthermalsci.2021.107053

[38] Tao YB, You Y, He YL. Lattice Boltzmann simulation on phase change heat transfer in metal foams/paraffin composite phase change material. Appl Therm Eng. 2016; 93: 476-85. http://dx.doi.org/10.1016/j.applthermaleng.2015.10.016

[39] Incropera FP, Dewitt DP, Bergman TL. Fundamentals of Heat and Mass Transfer. Hoboken (NJ): John Wiley & Sons Inc.; 2006.

[40] Ranut P, Nobile E, Mancini L. High resolution X-ray microtomography-based CFD simulation for the characterization of flow permeability and effective thermal conductivity of aluminum metal foams. Exp Therm Fluid Sci. 2015; 67: 30-6. http://dx.doi.org/10.1016/j.expthermflusci.2014.10.018

[41] Pei X, Liu Y, Xue L, Song L, Rang T. A new determination method for the anisotropic permeability tensor based on the passive differential pressure ratio. Int Commun Heat Mass Transf. 2023; 140: 106544. https://doi.org/10.1016/j.icheatmasstransfer.2022.106544

[42] Medraj M, Baril E, Loya V, Lefebvre LP. The effect of microstructure on the permeability of metallic foams. J Mater Sci. 2007; 42: 4372-83. https://doi.org/10.1007/s10853-006-0602-x

[43] Dukhan N, Minjeur CA II. A two-permeability approach for assessing flow properties in metal foam. J Porous Mater. 2011; 18: 417-24. https://doi.org/10.1007/s10934-010-9393-1

[44] Scandelli H, Ahmadi Senichault A, Levet C, Lachaud J. Computation of the Permeability Tensor of Non Periodic Anisotropic Porous Media from 3D Images. Transp Porous Med. 2022; 142: 669-97. https://doi.org/10.1007/s11242-022-01766-8

[45] Naldi C, Dongellini M, Morini GL. The evaluation of the effective thermal conductivity of metal-foam loaded phase change materials. J Energy Storage. 2022; 51: 104450. https://doi.org/10.1016/j.est.2022.104450

[46] Peng W, Xu M, Li X, Huai X, Liu Z, Wang H. CFD study on thermal transport in open-cell metal foams with and without a washcoat: Effective thermal conductivity and gas-solid interfacial heat transfer. Chem Eng Sci. 2017; 161: 92-108. http://dx.doi.org/10.1016/j.ces.2016.12.006

[47] Yang H, Li Y, Yang Y, Chen D, Zhu Y. Effective thermal conductivity of high porosity open-cell metal foams. Int J Heat Mass Transf. 2020; 147: 118974. https://doi.org/10.1016/j.ijheatmasstransfer.2019.118974

[48] Jayakumar A, Mani A. Image-based method for evaluation of effective thermal conductivity of metal foam with hollow ligaments. Int J Heat Mass Transf. 2021; 164: 120490. https://doi.org/10.1016/j.ijheatmasstransfer.2020.120490

[49] Bodla KK, Murthy JY, Garimella SV. Resistance network-based thermal conductivity model for metal foams. Comput Mater Sci. 2010; 50: 622-32. https://doi.org/10.1016/j.commatsci.2010.09.026

[50] Demir H, Mobedi M, Ülkü S. The use of metal piece additives to enhance heat transfer rate through an unconsolidated adsorbent bed. Int J Refrig. 2010; 33(4): 714-20. https://doi.org/10.1016/j.ijrefrig.2009.12.032